Mon. Not. R. Astron. Soc. **000**, 000–000 (0000) Printed 7 September 2010 (MN LATEX style file v2.2)

H-ATLAS: PACS imaging for the Science Demonstration Phase

Edo Ibar,[1] R. J. Ivison,[1,2] A. Cava,[3] G. Rodighiero,[4] S. Buttiglione,[5] P. Temi,[6] D. Frayer,[7] J. Fritz,[8] L. Leeuw,[6] M. Baes,[8] E. Rigby,[9] A. Verma,[10] S. Serjeant,[11] T. Müller,[12] R. Auld,[13] A. Dariush,[13] L. Dunne,[9] S. Eales,[13] S. Maddox,[9] P. Panuzzo,[14] E. Pascale,[13] M. Pohlen,[13] D. Smith,[9] G. de Zotti,[5,15] M. Vaccari,[4] R. Hopwood,[11] A. Cooray,[16] D. Burgarella[17] and M. Jarvis[18]

[1] *UK Astronomy Technology Centre, Royal Observatory, Blackford Hill, Edinburgh EH9 3HJ*
[2] *Institute for Astronomy, University of Edinburgh, Royal Observatory, Edinburgh EH9 3HJ*
[3] *Instituto de Astrofísica de Canarias and Departamento de Astrofísica de la Universidad de La Laguna, La Laguna, Tenerife, España*
[4] *University of Padova, Vicolo Osservatorio 3, I-35122, Padova, Italy*
[5] *INAF-Osservatorio Astronomico di Padova, Vicolo Osservatorio 5, I-35122, Padova, Italy*
[6] *Astrophysics Branch, NASA Ames Research Center, MS 245-6, Moffett Field, CA 94035, USA*
[7] *Infrared Processing and Analysis Center, California Institute of Technology 100-22, Pasadena, CA 91125, USA*
[8] *Sterrenkundig Observatorium, Universiteit Gent, Krijgslaan 281 S9, B-9000 Gent, Belgium*
[9] *School of Physics and Astronomy, University of Nottingham, Nottingham NG7 2RD*
[10] *Oxford Astrophysics, Denys Wilkinson Building, University of Oxford, Keble Road, Oxford OX1 3RH*
[11] *Dept. of Physics and Astronomy, The Open University, Milton Keynes MK7 6AA*
[12] *Max-Planck-Institut für extraterrestrische Physik, Giessenbachstrasse, 85748 Garching, Germany*
[13] *School of Physics and Astronomy, Cardiff University, Queens Buildings, The Parade, Cardiff CF24 3AA*
[14] *CEA, Laboratoire AIM, Irfu/SAp, F-91191 Gif-sur-Yvette, France*
[15] *SISSA, Via Bonomea 265, I-34136 Trieste, Italy*
[16] *Department of Physics and Astronomy, University of California, Irvine, CA 92697, USA*
[17] *Laboratoire d'Astrophysique de Marseille, Observatoire Astronomique Marseille Provence, Aix-Marseille Université, CNRS, France*
[18] *Centre for Astrophysics Research, STRI, University of Hertfordshire, Hatfield AL10 9AB*

Accepted 2010 August 27. Received 2010 August 26; in original form 2010 June 8

ABSTRACT

We describe the reduction of data taken with the PACS instrument on board the *Herschel Space Observatory* in the Science Demonstration Phase of the *Herschel*-ATLAS (*H*-ATLAS) survey, specifically data obtained for a 4×4-deg^2 region using *Herschel*'s fast-scan ($60\,\mathrm{arcsec\,s^{-1}}$) parallel mode. We describe in detail a pipeline for data reduction using customised procedures within HIPE from data retrieval to the production of science-quality images. We found that the standard procedure for removing Cosmic-Ray glitches also removed parts of bright sources and so implemented an effective two-stage process to minimise these problems. The pronounced $1/f$ noise is removed from the timelines using 3.4- and 2.5-arcmin boxcar high-pass filters at 100 and 160 μm. Empirical measurements of the point-spread function (PSF) are used to determine the encircled energy fraction as a function of aperture size. For the 100- and 160-μm bands, the effective PSFs are $\sim$9 and $\sim$13 arcsec (FWHM), and the 90-per-cent encircled energy radii are 13 and 18 arcsec. Astrometric accuracy is good to $\lesssim$2 arcsec. The noise in the final maps is correlated between neighbouring pixels and rather higher than advertised prior to launch. For a pair of cross-scans, the 5-σ point-source sensitivities are 125–165 mJy for 9–13-arcsec-radius apertures at 100 μm and 150–240 mJy for 13–18-arcsec-radius apertures at 160 μm.

Key words: Instrumentation – Data reduction

1 INTRODUCTION

The 3.5-m *Herschel Space Observatory*[1] (Pilbratt et al. 2010) is the first space telescope to cover the entire far-infrared waveband (from

[1] *Herschel* is an ESA space observatory with science instruments provided by European-led Principal Investigator consortia and with important participation from NASA.

55 to 670 μm) and looks likely to become one of the greatest astronomical achievements of this decade.

The *Herschel* Astrophysical Terahertz Large Area Survey (*H*-ATLAS – Eales et al. 2010) is the largest *Herschel* Open Time Key Project (600 hr), covering 550 deg^2 of sky in regions selected on the basis of existing multi-wavelength coverage (e.g. the Galaxy Evolution Explorer – GALEX, the Galaxy and Mass Assembly spectroscopic survey – GAMA, the 2dF Galaxy Redshift Survey – 2DFGRS, the Sloan Digital Sky Survey – SDSS, and the Dark Energy Survey – DES). *H*-ATLAS will detect hundreds of thousands of galaxies (Clements et al. 2010), and provide an extensive census of dust-obscured activity in the local ($z < 0.3$) Universe (Amblard et al. 2010). The areal coverage of *H*-ATLAS also makes it well suited to the identification of *Planck* sources (e.g. González-Nuevo et al. 2010), lensed galaxies at high redshift (e.g. Negrello et al. 2007; Swinbank et al. 2010) and local dust clouds at high Galactic latitudes; there is also enormous potential for serendipitous discovery.

H-ATLAS is exploiting the fast-scan (60 arcsec s^{-1}) parallel mode of *Herschel*, using two of the on-board instruments to provide an efficient way to map large areas of sky in five wavebands simultaneously. We are using the Photodetector Array Camera and Spectrometer (PACS – Poglitsch et al. 2010) to observe at 100 and 160 μm (its 'green' and 'red' channels) whilst the Spectral and Photometric Imaging Receiver (SPIRE – Griffin et al. 2010) is taking data at 250, 350 and 500 μm.

This paper is one of a series of four technical papers describing our approach to the PACS (this paper) and SPIRE (Pascale et al., in preparation) data products, to source extraction (Rigby et al., in preparation) and to cross-identification (Smith et al., in preparation) for the Science Demonstration Phase (SDP) of the *H*-ATLAS survey. These data are public and available at `http://www.h-atlas.org/`. Here, we describe the pipeline used to reduce data obtained with PACS, and the quality of data products, to give an idea of its scientific potential. In §2, we provide a brief description of the instrument; in §3, we present the *H*-ATLAS SDP observations; in §4, we describe the customised procedures we have developed within the *Herschel* Interactive Processing Environment (HIPE[2] – Ott 2010) to reduce data from PACS. In §5 we describe tests of the resulting images and we state some concluding remarks in §6.

2 PACS INSTRUMENT

PACS is a multi-colour camera and low- and medium-resolution spectrometer covering the 55–210-μm wavelength range (see Fig. 1). It comprises four large-format detector arrays: two filled silicon bolometer arrays optimised for imaging in high-photon-background conditions and two Ge:Ga photo-conductor arrays for spectroscopy. Here we concentrate on the bolometer detectors used by the *H*-ATLAS survey – a more complete description of the instrument and its modes can be found at Poglitsch et al. (2010). A dichroic beam splitter enables photometry in two bands simultaneously – 70 or 100 μm ('blue' or 'green', selected by a filter wheel) and 160 μm ('red') – over the same 1.75×3.5-arcmin^2 field of view. The bolometer arrays comprise 64×32 and 32×16 pixels, with 3.2 and 6.4 arcsec pixel^{-1} on-sky, respectively, providing close-to Nyquist beam sampling for the blue/green and red filters. The arrays each comprise sub-arrays of 16×16 pixels, tiled together to form the focal plane (see Billot et al. 2009 and references therein).

Working in 'scan mode', PACS modulates the sky signal by making use of the motion of the spacecraft (10, 20 or 60 arcsec s^{-1}), with no chopping. The sky signal is stored in units of mV by the analogue-to-digital (ADU) converter, depending on the user-defined V/ADU gain value (high or low; see Poglitsch et al. 2010). The signal from each bolometer pixel is sampled at a rate of 40 Hz, although due to satellite telemetry limitations, in scan mode the signal is averaged into packages of four consecutive frames – i.e. resulting in an effective rate of 10 Hz. Data is also bit-rounded by the Signal-Processing Unit (SPU) (Ottensamer & Kerschbaum 2008) which results in a stronger quantisation of the signal than would be expected by the ADU converter. When using the SPIRE/PACS 'fast-scan parallel mode', as employed by *H*-ATLAS, in particular for the blue/green filters, data suffer additional in-flight averaging (eight frames), resulting in an effective read-out frequency of 5 Hz.

Due to the limited signal bandwidth of the detection chain, the on-board data compression produces significant degradation of the observed point spread function (PSF; Instrument Control Centre – ICC report[3]). Simulated parallel mode data based on PACS prime fast-scan observations show that point-source peak fluxes are reduced by ∼50 and 70 per cent, at 100 and 160 μm respectively, in comparison to nominal (20 arcsec s^{-1}) scan observations[4] (Poglitsch et al. 2010).

Prior to assessment of the in-flight performance, the predicted 5-σ point-source *H*-ATLAS sensitivities based on the *Herschel*-Spot (HSpot[5]) observation planning tool were 67 and 94 mJy for observations with one pair of cross-scans, at 100 and 160 μm, respectively (Eales et al. 2010). The performance is mostly dependent on the optical efficiency, the thermal and telescope background, the effects of Cosmic-Ray glitches – in particular high-energy protons – and the photon noise from the detector and multiplexer electronics which was found to introduce a $1/f$ excess below 1 Hz prior to launch (see § 4.4).

The PACS focal plane is offset with respect to SPIRE by a fixed separation of ∼21 arcmin along the spacecraft z-axis, implying different instantaneous PACS and SPIRE coverages. The coverage obtained by SPIRE in the SDP area is presented in § 4.4 and clearly show that parallel mode is only efficient for large surveyed areas. For this mode, the angle between the spacecraft z-axis and the scan direction is either +42.4 or −42.4 deg in order to obtain an uniform coverage for SPIRE (see PACS Observer's Manual[6])

3 PACS *H*-ATLAS SDP DATA

On 2009 November 22 (Observing Day – OD 192) *Herschel* observed one of the equatorial fields of the *H*-ATLAS survey (see

[2] HIPE is a joint development by the *Herschel* Science Ground Segment Consortium, consisting of ESA, the NASA *Herschel* Science Center, and the HIFI, PACS and SPIRE consortia. HIPE is a graphical application which includes Jython scripting, data analysis, plotting, communication with the *Herschel* Science Archive and much more. Throughout the paper we refer to version 3.0.859, which is the build we used to reduce the *H*-ATLAS PACS SDP data. Note that HIPE is under continuous development.

[3] PICC-NHSC-TR-011, June 2008, version 0.3. Report by N. Billot et al.
[4] PICC-ME-TN-033, November 10, 2009, version 0.3 report by D. Lutz
[5] `herschel.esac.esa.int/Tools.shtml`
[6] `herschel.esac.esa.int/Docs/PACS/pdf/pacs_om.pdf`

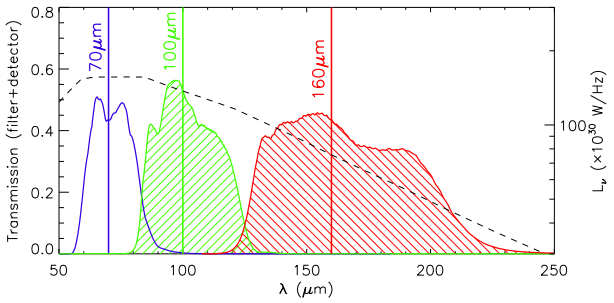

Figure 1. Transmission filter/detector profiles for the PACS 55–85- (blue), 85–125- (green) and 125–210-μm (red) passbands. The filled profiles show the filters used for the *H*-ATLAS observations (green and red). The dashed line shows the Spectral Energy Distribution (SED) of M 82 with units on the right-hand axis.

Table 1 of Eales et al. 2010). Observations covered an area of approximately $4\times4\,\mathrm{deg}^2$ (a quarter of the GAMA-A – also called the GAMA-9h – field). These constitute the *H*-ATLAS SDP observations (see Table 1).

Of the two available combinations of photometric bands for PACS, we opted to observe at 100 and 160 μm (see Fig. 1) because these are best suited to our science goals. Approximately 44 Gbytes of data were retrieved using HIPE via the *Herschel* Science Archive (HSA) interface.

One pair of cross-scans were taken, covering the entire $4\times4\,\mathrm{deg}^2$ field. The two resulting datasets (Observation ID – OBSID 1342187170 and 1342187171) comprise 89 and 97 parallel scan-legs, respectively, each $\sim$4 deg in length, separated from each other by $\sim$2.6 arcmin. After completing a scan-leg, the telescope turns around and performs the next parallel scan in the opposite direction. Every ten scan-legs, approximately, calibration observations are made to track any drifts in detector response: the telescope chops in a stationary position at the edge of the scan-leg for approximately half a minute (Krause et al. 2006). Given the in-flight stability of the PACS bolometers, the *Herschel* Science Centre (HSC) has decided to restrict calibration blocks to one per OBSID for the rest of *H*-ATLAS observations.

As well as ensuring good coverage of the field, the acquisition of two independent cross-scan measurements allows us to identify and remove drifts in the data timelines[7] and to use maximum-likelihood imaging algorithms (e.g. Cantalupo et al. 2010, Patanchon et al. 2008) which can help to mitigate the strong $1/f$ noise present in the data (see § 4.4.2).

4 THE PIPELINE

Our data analysis faced a significant computational challenge. To process the full pipeline and given by the particularly large data set, one must set up HIPE to increase the available random-access memory (RAM) limits to 60 Gbytes (or more). Within HIPE, the pipeline is written in Jython (a Python implementation written in Java) and consists of a series of tasks developed by the PACS ICC in collaboration with the HSC. HIPE allows the user to specify data-reduction steps, from data retrieval to the final imaging processes.

Thanks to the development of HIPE, the data processing is relatively straightforward. Nevertheless, it needs to be fine-tuned to deal effectively with cosmic-ray (CR) removal (deglitching – see § 4.3), and to perform the imaging necessary to tackle $1/f$ noise. A schematic view of the full pipeline is shown in Fig. 2.

[7] `herschel.esac.esa.int/Docs/PMODE/html/parallel_om.html`

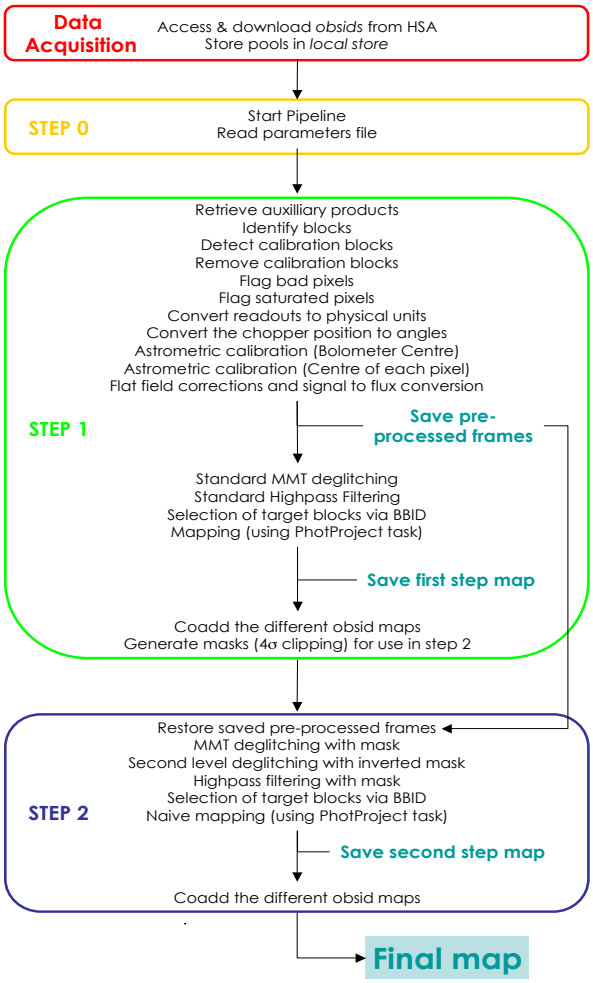

Figure 2. A flow-chart of the pipeline used for the PACS data reduction.

4.1 Retrieve and organise the data

The raw (so-called 'level-0') data were retrieved using HIPE task `getObservation` and saved into the local pool. These data contain all the information necessary for their reduction – science data as well as all the necessary housekeeping/auxiliary/calibration data.

The signal detected by the bolometers as a function of time (also named timeline frames) are extracted from the raw data and analysed carefully throughout the pipeline. We next extract the telemetry of the telescope contained in the pointing product, tables of the most up-to-date calibration values based on in-flight performance tests (extracted from the HIPE built using `getCalTree`) and the housekeeping data which tracks temperature and general instrument/telescope status.

An organisational task (`findBlocks`) is used to identify all the different types of data within the timeline frames. In particular, we remove the calibration blocks from the science frames using `detectCalibrationBlock` and `removeCalBlocks`, neglecting any temporal variation of the detector responsivity.

Proposal	Target	Scan	R.A. (J2000) (h:m:s)	Dec. (J2000) (°:":')	Observing date (y-m-d)	UT start time (h:m:s)	Duration (h)	OBSID
SDP_seales01_6	ATLAS_SDn	Nominal	09:05:30.0	+0:30:00.0	2009-11-22	00:18:02.392	8.11261	1342187170
SDP_seales01_6	ATLAS_SDn	Orthogonal	09:05:30.0	+0:30:00.0	2009-11-22	08:24:55.277	8.05333	1342187171

Table 1. The fast-scan parallel mode SDP observations ($4\times4\,\mathrm{deg}^2$) for the *H*-ATLAS survey.

4.2 Flagging and calibration

This data-processing stage is described in the PACS Data Reduction Manual[8] and it is almost user-independent.

First, those bolometers identified as corrupt in ground-based tests are removed using `photFlagBadPixels`, while saturated pixels are masked with `photFlagSaturation`. These two tasks mask approximately 2–3 per cent of the bolometers and result in no significant loss in areal coverage.

The raw signal measured by each bolometer ($S_{\rm ADU}$) is quantified in steps of 2×10^5 V as determined by the gain and the bit-rounding applied to the fast-scan parallel-mode data. We use `photConvDigit2Volts` to transform ADU signals into Volts. Possible cross-talk in the multiplexed readout electronics has not been taken into account. We set the chopper angle with `convertChopper2Angle` (set to zero while scanning) in order to obtain the instantaneous PACS line of sight with respect to the spacecraft line of sight, and to facilitate the coordinate determination for a reference pixel using the task `photAddInstantPointing`. Then, using `photAssignRaDec`, we define the astrometric calibration for every pixel in the PACS bolometer arrays.

Having flagged the timelines, converted the units to Volts and calibrated astrometrically, we apply a flat-field correction using `photRespFlatfieldCorrection`. This task is used to convert the signal into flux density units, making use all the available calibration products from the *Herschel* campaign. In our data processing, we have used the default calibration tree from the HIPE v3.0.859 build. In particular we use the version-3 `responsivity` file that is known to be slightly biased. See later in §5.2, where we describe the correction factors required to obtain good flux calibration.

At this stage – for the sake of efficiency – we save the pre-processed frames, before re-using them in the upcoming deglitching and high-pass filtering tasks.

4.3 Deglitching

As already noted, the process of identifying and removing glitches needs to be fine-tuned during the data processing. In this section we describe the routines developed to take into account hits by CRs on the detectors.

4.3.1 Classes of observed glitches

By inspecting the timelines, it is possible to identify two main types of glitches.

First, single-pixel/single-frame glitches: these are similar to those found in optical images, in the sense they appear in just one frame (i.e. one read-out in the timeline) and they affect only one bolometer of the detector array. We show a green bolometer's timeline displaying such glitches in Fig. 3 (top panel). Glitches of this type are seen as single points, lying clearly above (or below) the average timeline values.

In order to mask these glitches we make use of the Multi-resolution Median Transform (MMT – Starck & Murtagh 1998) approach (task provided within HIPE – `photMMTDeglitching`) which performs an analysis of the signal along each bolometer's timeline to identify outliers produced by CR impacts. Fig. 3 shows a typical example for the effect that `photMMTDeglitching` has on the timelines (top, original data; bottom, data after deglitching). For our *H*-ATLAS observations, we used the following parameters for this task, `scales=3` and `sigma=5`, which were found to remove single-pixel/single-frame glitches efficiently.

Secondly, multi-pixel/multi-frame glitches: these are easily recognisable in a timeline since they are characterised by a sudden increase (decrease) in signal, which reaches a level well above (below) the average within one or two frames, followed by an exponential decrease (increase) that varies in character from event to event (see green ellipses in Fig.3).

The inset in the top panel of Fig. 3 shows (in red) how a full bolometer sub-array is affected by a multi-pixel/multi-frame glitch (green ellipses) and masked by MMT. Such events are likely due to a very energetic particle hitting the electronics, causing a sudden signal increase (or decrease) in an entire sub-array for $\sim$500 frames, thus potentially affecting regions as large as $\sim$2 deg in the projected images. Such glitches are not fully removed by the MMT task but are partially removed by an aggressive high-pass filter (§4.4.1).

4.3.2 Issues relating to the MMT task – masking

As already noted, the use of the MMT task for deglitching is an efficient way to remove single-pixel/single-frame glitches caused by CRs. However, an important drawback of this algorithm is that it can affect subsequent measurements of bright sources, i.e. sources whose flux densities are significantly higher than the mean background level. In Fig. 4 we illustrate this issue using one of the brightest sources in the *H*-ATLAS SDP field. The innermost brightest map pixels are masked and therefore they do not contribute to the observed flux density of the source. We proved that it is impossible to tune the `photMMTDeglitching` parameters to remove glitches effectively whilst maintaining the signal from bright sources. Indeed, the timeline behaviour for a point source observed in fast-scan parallel mode is almost indistinguishable from a glitch because the effective sampling rate of 5 and 10 Hz corresponds to scales of 12 and 6 arcsec when moving at 60 arcsec s^{-1} for the green and red data, respectively. These scales are similar to the observed PSFs, therefore bright point sources resemble single-pixel/single-frame glitches – especially in the green data.

To avoid removing flux from real sources we employ a 2nd-level stage in the deglitching process. First, we project the time-

[8] `herschel.esac.esa.int/Data_Processing.shtml`

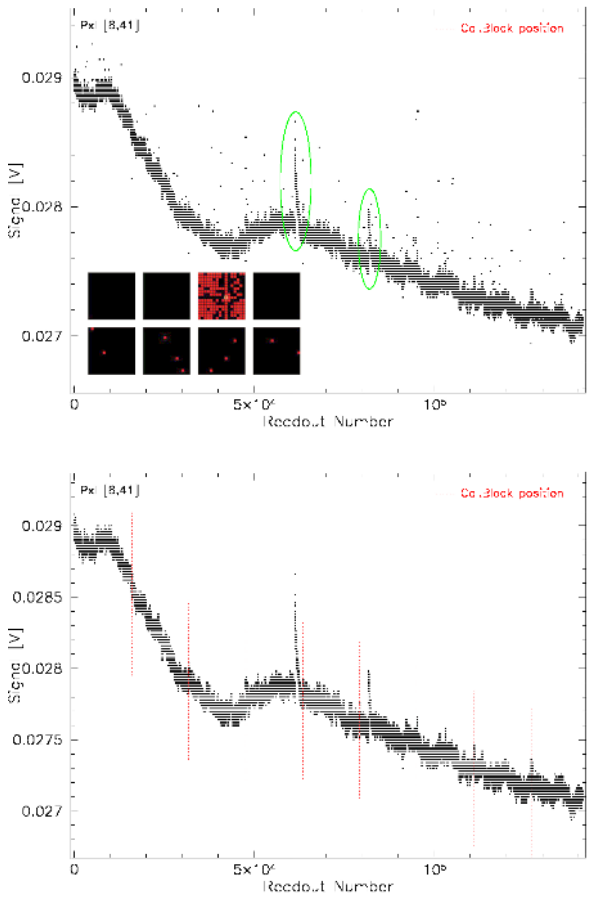

Figure 3. Example of a timeline for a green bolometer (8,41) in the *H*-ATLAS SDP data, before (top panel) and after (bottom panel) glitch removal. Green ellipses show two multi-pixel/multi-frame glitches. Red dotted lines show the timeline locations for calibration blocks (not associated to the glitches). The small sketch on the top figure shows the PACS bolometer pixels being simultaneously flagged by MMT (in red) due to a multi-pixel/multi-frame glitch.

lines to generate an image (see § 4.4.1) to identify all the map pixels where the signal is higher than $4\,\sigma$ (the pixel r.m.s. is determined from a $0.2\,\mathrm{deg}^2$ region devoid of bright sources). Next, we use `photReadMaskFromImage` to create a mask for all those frames contributing at these masked positions. This mask allows us to run `photMMTDeglitching` again, this time avoiding all those frames that contribute to the masked pixels, thus avoiding real sources. In this way, MMT removes the vast majority of the low-energy CR hits from the data.

Glitches powerful enough to create $>4\,\sigma$ events in the aforementioned image can be identified easily as outliers in the signals contributing to each individual pixel. We built an index map cube with `photProject` (`slimindex = False`) to identify the frames contributing to each map pixel (there are $\sim$15 and $\sim$30 frames per pixel for the 100- and 160-μm images, respectively), and make use of `IIndLevelDeglitchTask` to remove clear outliers from these contributions (we use `deglitchvector = 'framessignal'`). In `IIndLevelDeglitchTask`, the glitch detection threshold is set to $5\,\sigma$ using the `Sigclip` task.

To determine whether deglitching is removing flux from bright sources we employ a simple sanity check: we examine the coverage map at the those positions. In Fig. 4 (*right*), we show the resultant coverage maps after a simple run of `photMMTDeglitching` (top) and after applying 2nd-level deglitching aided by masks (bottom). The hole seen in the coverage represents data that have been removed by mistake during the deglitching phase. Using 2nd-level deglitching, this hole is significantly reduced.

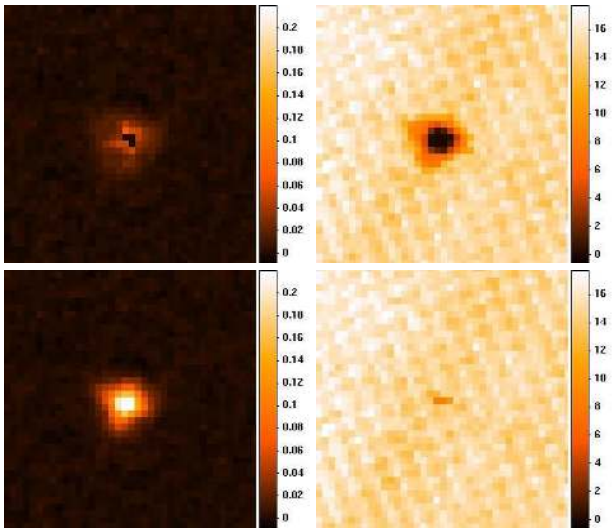

Figure 4. Images illustrating the importance of masking on 2nd-level deglitching. A bright 100-μm source image is shown to the left and its coverage maps (after deglitching process) to the right. The top panels show the removal produced by `photMMTDeglitching`, while the bottom ones show the same source but using the `IIndLevelDeglitchTask` approach. Image and coverage maps are in units of Jy/pixel (2.5 arcsec pix^{-1}) and frames per pixel scales, respectively.

We note this deglitching approach is still under development. We find that a small amount of data are still flagged erroneously (or leaving few remaining glitches) due to the high scatter produced by steep flux gradients when comparing the contributions to the very brightest map pixels.

As we have shown, we find that an effective way to treat glitches is with a combination of the two aforementioned tasks: `photMMTDeglitching` on the background, followed by `IIndLevelDeglitchTask` on the possible sources, aided by source masks in both cases – see Fig. 2 as our recommended guide.

4.4 Imaging

Within HIPE, there are two possible ways to project the timelines of scan-mode observations. First, a simple (also called 'naïve' or drizzle) projection (`photProject`; see § 4.4.1) on sky for every frame – simply dividing and weighting the signal according to the projection of each bolometer onto a pixelated sky (Fruchter & Hook 2002, Serjeant et al. 2003). Given the pronounced $1/f$ noise (see Fig. 5), an aggressive high-pass filter has to be applied to the timelines for this task to work efficiently. Second, the Microwave Anisotropy Dataset mapper (MADmap – `runMadMap`) can be also used (Cantalupo et al. 2010, and see §4.4.2). This task uses a maximum-likelihood map reconstruction algorithm, which requires good knowledge of the noise but does not require aggressive high-pass filtering. For the SDP data, we opted to run the naïve projection.

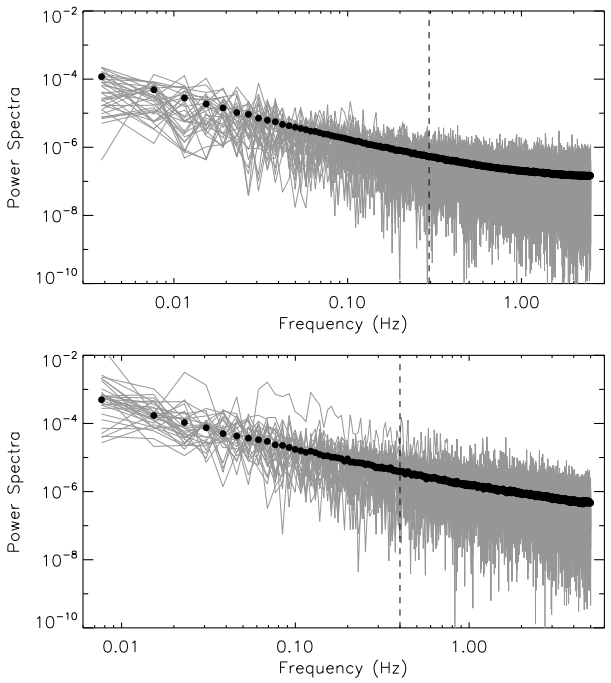

Figure 5. The thick black dots show the median power spectrum for a single scan leg (4 deg) obtained from the bulk (32×64 for green and 16×32 for red) of the bolometer timelines (after deglitching). The top and bottom panels show the typical 100- and 160-μm power spectra (in arbitrary units), respectively. Some few individual power spectra are shown with grey lines to visualise the scatter. The $1/f$ signature is evident on the data. The length of the high-pass filters described on § 4.4.1 (3.4 and 2.5 arcmin for green and red timelines, respectively) are shown in terms of frequency by vertical dashed lines.

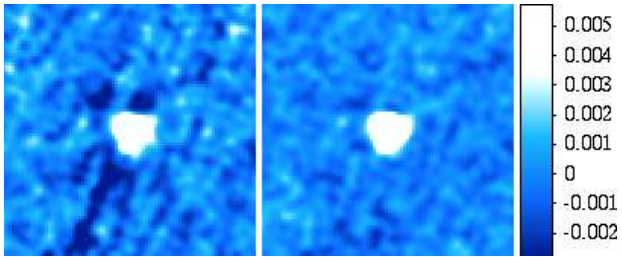

Figure 6. Left: the effect of aggressive high-pass filtering seen around a bright 100-μm source along the scan direction. Right: masking correction applied by the 2nd-level high-pass filtering approach. The colour scale is in Jy pixel^{-1}, where the pixel scale is 2.5 arcsec. Note that the higher noise in the left image is the result of an earlier data reduction with an older HIPE built (for displaying purposes only).

4.4.1 *Naïve projection*

As already mentioned, in order to remove the thermal drifts from the timelines, we have applied a boxcar high-pass filter (`highpassFilter` – HPF) on a length scale of 15 [3.4] and 25 [2.5] frames [arcmin] to the 100- and 160-μm timelines, respectively (note these scales correspond to $2 \times \mathrm{D} + 1$ where D is the input value to run the task). The HPF subtracts a running median from each readout frame, thereby removing all the large-scale structure from the map, including thermal drifts, cosmic cirrus and extended sources – this naïve projection is only efficient to detect point-like sources.

This aggressive high-pass filtering inevitably results in an under-estimation of peak flux densities. Indeed, around bright sources negative sidelobes are seen clearly along the scan-direction (see Fig. 6-left). For this reason, we have used the so-called '2nd-level high-pass filtering' approach, which basically avoid a biased median subtraction due to the presence of strong signals on the timelines (due to real sources). We use the same mask created for the 2nd-level deglitching, i.e. flagging those timeline frames contributing to all 4-σ map pixels, in order to not to bias the median boxcar high-pass filter estimate (`maskname` keyword within `highpassFilter`). In Fig. 6-right we clearly show the improvement made by this '2nd-level high-pass filtering' which is specially important to co-add different scans and maintain an uniform PSF across the map.

Finally, just before producing the final images using `photProject` we select only those frames which were used for scanning the target GAMA field (i.e. removing turnarounds and remaining calibration blocks) via the Building Block ID (`BBID = 215131301`) number.

The resultant maps were chosen to have 2.5- and 5.0-arcsec pixel sizes for the green and red filters, respectively. These sizes were chosen in consultation with the *H*-ATLAS SPIRE data reduction group (Pascale et al., in prep.) and ensure that all five images can be combined trivially (the pixel scales are 5, 10 and 10 arcsec at 250, 350 and 500 μm, respectively). The full PACS cross-scan coverage (top) and a small sub-region (bottom – a tenth of the full image) are shown in Fig. 7.

4.4.2 *MADmap imaging*

Although naïve maps are well-suited to our early SDP science goals, maximum-likelihood map-makers are required to recover large-scale diffuse emission, like Galactic cirrus and/or extended local galaxies. Here, we describe modest progress with the MADmap imaging task (`runMadMap`) implemented within HIPE.

If observations contain a good mix of spatial and temporal information at any given point on the sky, MADmap can aid in the removal of uncorrelated low-frequency noise (Waskett et al. 2007). We have combined the two SDP scans (obtained $\sim$8 hr apart; Table 1) to produce an image that suffers less from the pronounced drifts generated by the $1/f$ noise (see Fig. 5). In order to successfully solve this inversion method, a good characterisation of the noise must be provided to MADmap (see Cantalupo et al. 2010). This requires that correlated noise amongst detectors, and other correlated artifacts, must be removed from the data, or at least mitigated.

Fig. 8 shows how MADmap improves the recovery of extended emission, avoiding the loss of signal which results from the high-pass filter required for naïve projection. The images show a bright, extended source (J090402.9+005436; Thompson et al., in preparation). The MADmap images have a smoother background than those produced using `photProject`. However, we find that MADmap projection is sensitive to the sudden jumps produced by multi-pixel/multi-frame glitches, and by the long thermal drifts observed after calibration blocks (correlated features). In the future we will present a more detailed pre-processing analysis required to use MADmap within HIPE, and explore other approaches for imaging.

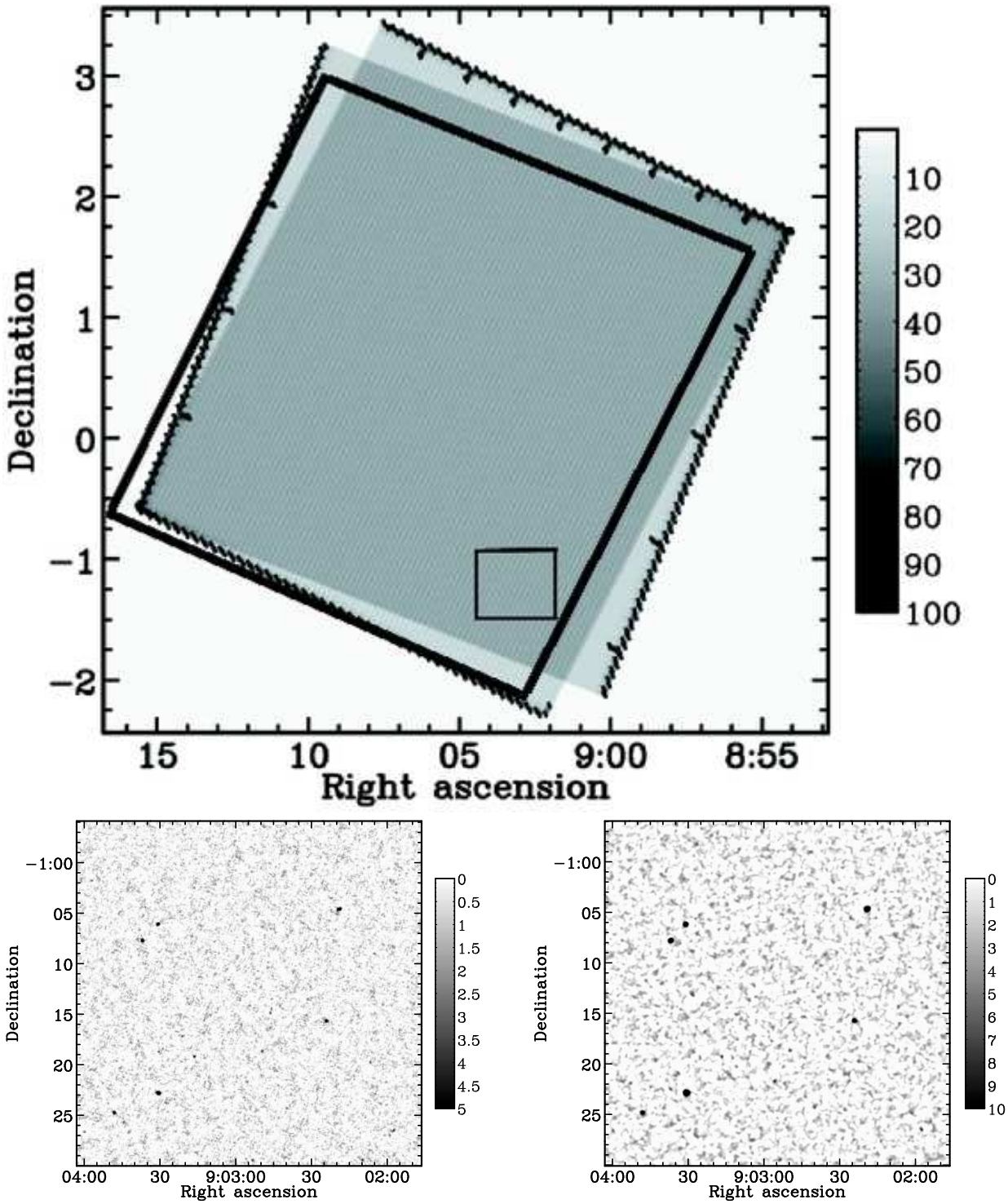

Figure 7. Top: full PACS coverage for the $4\times4\,\mathrm{deg}^2$ *H*-ATLAS SDP observations in units of frames per pixel (at 160 μm). The large, thick square shows the SPIRE coverage ($\sim$21 arcmin offset). Bottom: a small $\sim 0.4^2\,\mathrm{deg}^2$ region of the field (small, thin square in top figure) centred at R.A. = 9h 2m 54.5s and Dec. = $-01^\circ\,12''\,54.5'$ imaged at 100 (left) and 160 μm (right). The bottom images have been convolved with a 2-pixel-wide Gaussian (pixels of 2.5 and 5.0 arcsec for green and red, respectively) for display purposes.

5 IMAGE ANALYSES

5.1 Point-spread function

The observed PSF in fast-scan parallel mode ($60\,\mathrm{arcsec\,s}^{-1}$) suffers from strong smearing effects due to the averaged sampling frequency and the detector time constant which results in an elongation of the PSF in the direction of the scan. The expected FWHM broadening factors are $\sim$1.9 and $\sim$1.4 with respect to that observed using nominal scan speed ($20\,\mathrm{arcsec\,s}^{-1}$) at 100 and 160 μm, respectively (see ICC report in footnote 4 for more details). The PSF

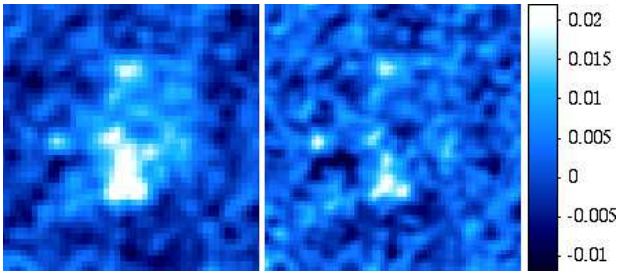

Figure 8. *Left:* an extended 160-μm source, imaged using MADmap (`runMadMap`); *right:* the same source imaged using `photProject`. Colour scale in Jy pixel^{-1} (though we have not fully tested calibration of the MADmap images). The recovery of extended emission in the MADmap image is evident.

shape becomes even more complicated when combining different scan directions. We have roughly modelled the PSF based on observations to the Vesta (OD160) asteroid (provided by ICC). We take this image and co-add it to the same image but rotated by 90° to simulate the cross-scanning. A 2-D Gaussian fit resulted in a FWHM of 8.7 and 13.1 arcsec at 100 and 160 μm, respectively.

In an attempt to measure the PSF using the bright sources in our final image product, we have stacked the PACS signal of 25 radio sources detected in the Faint Images of the Radio Sky at Twenty Centimeters (FIRST – Becker et al. 1995) survey. The measured FWHM of the stacked signal using a 2-D Gaussian fit results in 11.25×12.25 and 15×17.5 arcsec^2 at 100 and 160 μm, respectively. These are larger than the PSF produced from the Vesta images, which could be the result of slight pointing offsets, time shifts on science data, intrinsically extended and/or blended sources. Given these reasons and the uncertainty on the observed PSF, we have considered the fits provided by the PACS ICC (see footnote 4) to be inappropriate for our specific *H*-ATLAS analyses.

We have instead adopted an empirical approach to characterise the PSF. We use a bright, point-like source (flux densities of $S_{100\mu\mathrm{m}} = 7.5$ Jy and $S_{160\mu\mathrm{m}} = 2.9$ Jy) detected near the field centre of a calibration observation (OBSID 1342190267 and 1342190268) made in the α Bootes field. These data were observed in the same fast-scan parallel mode as our *H*-ATLAS data (with similar cross-scans) and reduced using exactly the same pipeline described in this paper. Using this bright source we are able to describe the radial profile of the PSF (and necessary aperture corrections) empirically, as shown in Fig. 9. We follow the same procedure as the PACS ICC, normalising our measures to a radius aperture of 60 arcsec, with background subtraction done in an annulus between radius 61 and 70 arcsec (effectively zero in our map). We find a good agreement between our 160-μm profile and that taken in slow-scan mode. As expected, we find evidence that small apertures under-estimate the encircled energy in fast-scan mode (especially for the green filter). With larger apertures we obtain smaller aperture corrections, indicating that our approach under-estimates the size of the PSF wings – standard empirical measurements could never detect the broad wings of the PSF. Fig. 9 is used for *H*-ATLAS source extraction, as described by Rigby et al. (in prep.).

5.2 Sensitivity of the maps

Several different calibration files have been implemented in HIPE. We use the default 'version 3' of the flux calibration files from HIPE v3.0.859 which have been found to be biased by the PACS

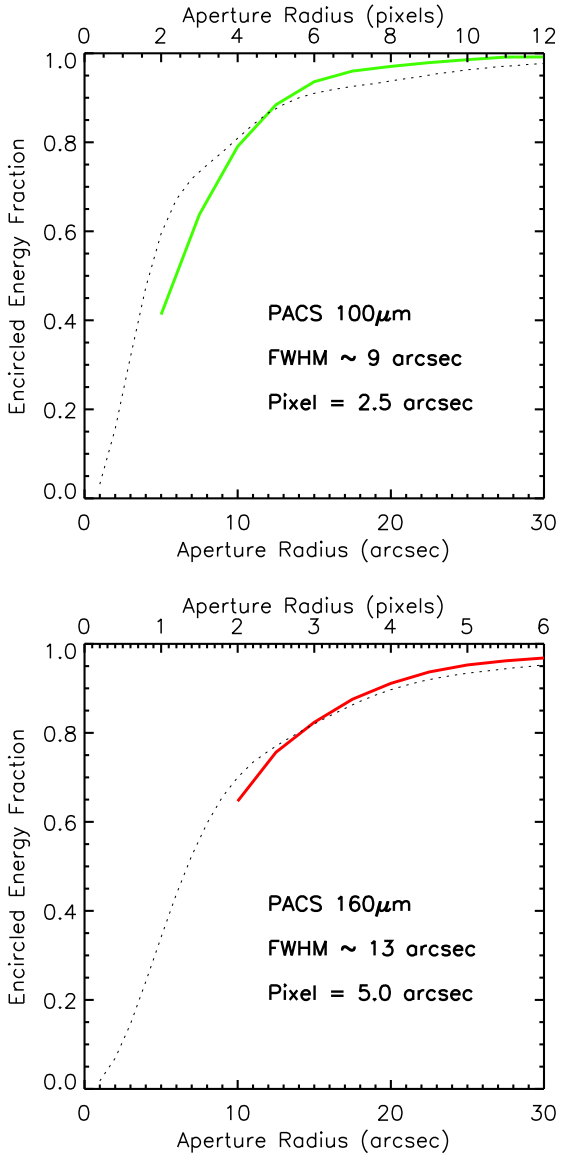

Figure 9. Encircled energy fraction normalised to an aperture of 60 arcsec (effectively zero background subtraction) as a function of aperture radius, in steps of 2.5 arcsec, for both PACS 100- (left) and 160-μm (right) passbands. The estimates are based on a bright point-like source found in an ICC calibration observations (OBSID 1342190267 and 1342190268) of α Bootes made in fast-scan SPIRE/PACS parallel mode, with two cross-scans. Dotted lines correspond to the ICC estimates, derived from slow-scan observations (OD160) of Vesta (normalised to a same 60 arcsec aperture). The quoted pixel-scales are the ones used for the map production.

ICC[9]. Flux densities have been found to be over-estimated by a factor of 1.09 (at 100 μm) and 1.29 (at 160 μm) with respect to previous observations by *Spitzer* and the *Infrared Astronomical Satellite (IRAS)*. These corrections are applied on the public release of these maps. The absolute calibration uncertainties measured by the ICC calibration campaign are currently within 10 and 20 per cent for the 100- and the 160-μm wavebands, respectively.

[9] PICC-ME-TN-035, February 23, 2010, version 1.1 report by The PACS ICC.

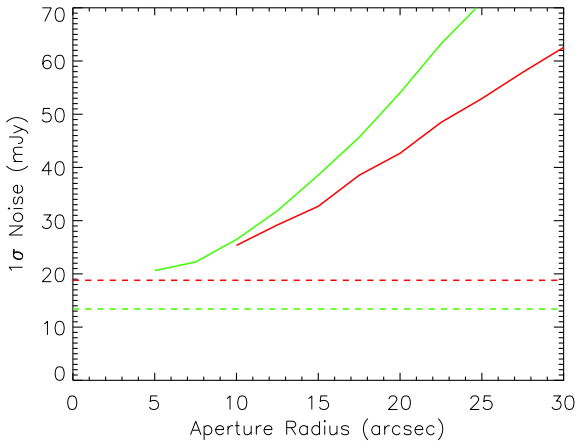

Figure 10. Continuum lines: noise estimates for the 100- (green) and 160-μm (red) images as a function of aperture size. Dashed lines: the 1-σ point-source sensitivities expected for *H*-ATLAS based on the HSpot observation planning tool (as shown in Eales et al. 2010).

To measure the noise in the maps we have used the aperture corrections from Fig. 9 in combination with the calibration correction factors stated above. We made aperture measurements at random locations within the central part of the image – placing apertures randomly and measuring counts within those apertures. To ensure that our noise measurements were not affected by sources, we made 10,000 aperture measurements, then carried out iterative clipping at the 2.5-σ level, where we take the median deviation measurements and throw out points more than $\pm 2.5\sigma$ from the median. We repeat this process until it converges – in typically 3–7 iterations. As a cross-check, we also fit a Gaussian to the clipped histogram of the data distribution (e.g. from -2.5- to 0.5- or 1-σ, re-deriving σ and repeating) which is better for confused maps. In this case, simple σ clipping and fitting the histogram distribution yield the same noise level. Given that the PACS data are filtered, the local background is fairly flat and we do not need to subtract a background torus for each of the measurements. These estimates are shown in Fig. 10.

We show the noise is strongly dependent on the aperture we use. Fig. 10 may suggest more correlated noise in the 100-μm data given the larger increase in noise as a function of spatial scale compared with the 160-μm data. We find that the 1-σ noise varies from 25 to 33 mJy for 9 to 13 arcsec, and from 30 to 48 mJy for 13 to 18 arcsec aperture radii for the 100- and 160-μm wavebands, respectively. These measurements are less sensitive than those predicted by HSpot (13.4 and 18.8 for green and red, respectively) and quoted in Eales et al. (2010). The sensitivities predicted by HSpot are based on the assumption that the noise power spectrum at 3 Hz should be white. In Fig. 5 we can clearly see that when we use a high-pass filter to tackle timeline drifts, the remaining noise at 3 Hz is not white: it includes other noise components that must reduce the sensitivity of the final images. A further analysis using a different imaging approach may be required.

5.3 Flux density calibration

We performed a sanity check on the flux calibration making use of photometric 100-μm IRAS coverage in the field. We select 14 IRAS sources (robustly detected at 100 μm) with clear detections in our PACS image. A full description of the source extraction for the *H*-ATLAS survey is presented in Rigby et al. (in preparation). For this test, we perform a source extraction using aperture photometry within SExtractor (`flux auto`) and correcting flux densities using Fig. 9. We find a bootstrapped median of $(S_{100-\mathrm{PACS}}/S_{100-\mathrm{IRAS}}) = 1.03 \pm 0.08$ for the flux density ratio. Despite the small number of sources, this roughly confirms the quality of the flux calibration within HIPE. According to an ICC report (footnote 9), these calibrations are still under development within HIPE.

Note that monochromatic flux densities quoted from broadband photometry are dependent on the shape of the SED (colour corrections). Indeed, based on the PACS filter profiles (see Fig. 1), small variations of the order of $\lesssim 5$ per cent have to be applied to the observed flux density at the reference wavelength. These variations are significant for cold ($<$20 K) sources (Poglitsch et al. 2010).

	R.A. offset (arcsec)	r.m.s. (arcsec)	Dec. offset (arcsec)	r.m.s. (arcsec)	N
100μm – 160μm	-0.5±0.1	1.2	1.3±0.1	1.4	94
100μm – SPIRE	-1.0±0.1	1.4	2.4±0.1	1.3	93
100μm – FIRST	-1.3±0.3	1.5	2.1±0.4	0.8	25
160μm – 100μm	0.5±0.1	1.2	-1.3±0.1	1.4	94
160μm – SPIRE	-0.6±0.2	1.8	1.1±0.1	1.5	138
160μm – FIRST	-0.8±0.3	1.8	0.8±0.2	1.1	29
SPIRE - FIRST	0.1±0.2	2.0	0.1±0.2	2.0	85

Table 2. A table summarising the mean astrometric offsets and r.m.s deviations between the PACS images and other catalogues. N stands for the number of matched sources. The SPIRE-FIRST comparison is included for completeness.

5.4 Astrometry

The pipeline-reduced maps are already astrometrically calibrated. We confirmed and checked the accuracy of the astrometric solution of the PACS green and red maps against the FIRST catalogue, the parallel SPIRE catalogue (Rigby et al., in preparation) and with respect to each other. Catalogue sources were deemed to be matches if an association was found within 6 arcsec. The mean offsets are summarised in Table 2 along with the number of matches between the input catalogues used to determine the offsets. The mean offsets and standard deviations are smaller than the search radius used for the matching. This, together with the negligible sub-pixel change in astrometric offset for association radii between 5 and 10 arcsec, supports the idea that the quoted offsets and standard deviations are representative of the astrometric accuracy of the maps. Both green and red maps were seen to be well aligned with each other and to the SPIRE and FIRST catalogues. An analysis of the direction of the offsets suggests that there is a systematic offset between the PACS green map and SPIRE catalogue of -1 and +2.4 arcsec in R.A. and Dec., respectively. This might be related to recent ICC findings relating to a 50-ms time shift in science data (T. Müller, priv. comm.). As all of the mean offsets are close to the size of a single PACS pixel (and significantly smaller than an individual SPIRE pixel – see § 4.4) we have not applied any global offsets to the maps but simply quote the offsets and accuracy between frames here.

6 CONCLUDING REMARKS

We have been able to produce science-quality images of a large ($4\times4\,\mathrm{deg}^2$) area of sky with the PACS instrument on board the *Herschel Space Observatory*. We describe the data processing implemented within HIPE and used to image the SDP region of the *H*-ATLAS survey. Data were taken in fast-scan ($60\,\mathrm{arcsec\,s}^{-1}$) parallel mode using PACS at 100 and 160 μm.

During the data reduction we faced many difficulties, principally due to the large volume of data. Only machines with at least 60 Gbytes of RAM were able to process the full data reduction. The pipeline was developed using customised HIPE procedures from data retrieval to final imaging (see Fig. 2). We describe an effective approach to tackle powerful glitches and the pronounced $1/f$ noise present in the data. We perform a careful analysis to protect the signal at the position of bright sources using masks during deglitching and filtering processes. In this early SDP data reduction, we cannot guarantee the complete absence of glitches in the image products. This could result in spurious sources, with obvious consequences when, e.g., determining accurate source counts or searching for outliers in flux or colours. The following *H*-ATLAS data releases will mitigate this problem.

Based on the final images, we describe the PSF, sensitivity, calibration and astrometric quality of the maps. In particular, we find previous HSpot sensitivities are too optimistic (see Fig. 10) compared to those measured in our maps. In principle, the origin of this discrepancy is unknown and further development of the pipeline may be required to allow us to reach a sensitivity closer to the instrumental noise expectations.

H-ATLAS PACS SDP products are avaiable at `http://www.h-atlas.org/`.

ACKNOWLEDGEMENTS

PACS has been developed by a consortium of institutes led by MPE (Germany) and including UVIE (Austria); KU Leuven, CSL, IMEC (Belgium); CEA, LAM (France); MPIA (Germany); INAFIFSI /OAA/OAP/OAT, LENS, SISSA (Italy); IAC (Spain). This development has been supported by the funding agencies BMVIT (Austria), ESA-PRODEX (Belgium), CEA/CNES (France), DLR (Germany), ASI/INAF (Italy), and CICYT/MCYT (Spain). We would like to thank the PACS-ICC team for providing excellent support to the *H*-ATLAS project and for the various HIPE developments that comprise the current pipeline. Finally, we thank the referee for comments that significantly improved this paper.

References

Amblard A. et al., 2010, A&A, 518, L9

Becker R. H., White R. L., Helfand D. J., 1995, ApJ, 450, 559

Billot N., Rodriguez L., Okumura K., Sauvage M., Agnèse P., 2009, in EAS Publications Series, Vol. 37, P. Kern , ed, EAS Publications Series, p. 119

Cantalupo C. M., Borrill J. D., Jaffe A. H., Kisner T. S., Stompor R., 2010, ApJS, 187, 212

Clements D. L. et al., 2010, A&A, 518, L8

Eales S. et al., 2010, PASP, 122, 499

Fruchter A. S., Hook R. N., 2002, PASP, 114, 144

González-Nuevo J. et al., 2010, A&A, 518, L38

Griffin M. J. et al., 2010, A&A, 518, L3

Krause O., Lemke D., Hofferbert R., Böhm A., Klaas U., Katzer J., Höller F., Salvasohn M., 2006, in Presented at the Society of Photo-Optical Instrumentation Engineers (SPIE) Conference, Vol. 6273, Society of Photo-Optical Instrumentation Engineers (SPIE) Conference Series

Negrello M., Perrotta F., González-Nuevo J., Silva L., de Zotti G., Granato G. L., Baccigalupi C., Danese L., 2007, MNRAS, 377, 1557

Ott S., 2010, in Y. Mizumoto, K.-I. Morita, & M. Ohishi , ed, ASP Conference Series, Astronomical Data Analysis Software and Systems XIX

Ottensamer R., Kerschbaum F., 2008, in Presented at the Society of Photo-Optical Instrumentation Engineers (SPIE) Conference, Vol. 7019, Society of Photo-Optical Instrumentation Engineers (SPIE) Conference Series

Patanchon G. et al., 2008, ApJ, 681, 708

Pilbratt G. L. et al., 2010, A&A, 518, L1

Poglitsch A. et al., 2010, A&A, 518, L2

Serjeant S. et al., 2003, MNRAS, 344, 887

Starck J., Murtagh F., 1998, PASP, 110, 193

Swinbank A. M. et al., 2010, Nature, 464, 733

Waskett T. J., Sibthorpe B., Griffin M. J., Chanial P. F., 2007, MNRAS, 381, 1583